Subject: Προώθ.: Geophysical Journal International - GJI-S-09-0595.R1
From: Andreas Skarlatoudis <askarlat@geo.auth.gr>
Date: Mon, 22 Mar 2010 15:48:54 +0200
To: kpapaza@geo.auth.gr, ntheo@itsak.gr

----- Προώθηση μηνύματος από vjd@ras.org.uk -----
Ημερομ.: Mon, 22 Mar 2010 09:17:11 -0400 (EDT)
Από: vjd@ras.org.uk
Απάντησηvjd@ras.org.uk
Θέμα: Geophysical Journal International - GJI-S-09-0595.R1
Προς: askarlat@geo.auth.gr
Προς: janet.marriott@wiley.com

Dear Dr. Skarlatoudis

I am pleased to inform you that your manuscript of ref. GJI-S-09-0595.R1 ["Local site-effects for the city of Thessaloniki (N. Greece) using a 3D Finite-Difference method: A case of complex dependence on source and model parameters"] has now been accepted for publication in Geophysical Journal International.

The editor comments: "
Editor: Korn, Michael
Comments to the Author:
(There are no comments)
"

The details are as follows:

Accepted 2010 March 22. Received 2010 March 04; in original form 2009 November 17 .

The paper contains 12 figures and 5 tables.

The following information is important; you should follow these instructions carefully.

There are certain administrative tasks that must be completed before your paper can be published. The Exclusive Licence Form (ELF) and (if your paper contains colour figures for publication in the paper version of the journal) the colour work agreement form are critical - Wiley-Blackwell WILL NOT PROCESS your paper until they receive them.

1. Exclusive Licence Form (ELF):

If you have not already done so, you must now complete the Exclusive Licence Form (ELF) available from http://www.blackwellpublishing.com/pdf/gji_caf.pdf and send a SIGNED copy to: The Production Editor, Geophys. J. Int., Wiley-Blackwell, 101 George Street, Edinburgh EH2 3ES, UK. Fax: 44 131 226 3803

Please mark the reference number of the paper on the form clearly.

2. Colour Figures:

Colour on the web is free, but if you have colour figures for publication in the paper issue of GJI, the cost will be £135 VAT per paper, regardless of the number of colour figures. In this case, you must complete the colourwork agreement form which is available from http://www.blackwellpublishing.com/pdf/gji_form.pdf. The completed and signed form should be sent to: The Production Editor, Geophys. J. Int., Wiley-Blackwell, 101 George Street, Edinburgh EH2 3ES, UK. Fax: 44 131 226 3803

Please mark the reference number of the paper on the form clearly.

If you wish us to publish colour versions of your figures on the web only, you should already have provided us with both grey scale and colour versions of your figures in electronic form (TIFF, PS or EPS). Your paper will appear with colour figures in the

electronic versions (html and .pdf) of the journal and grey scales in the paper version. If you wish to take up this option, and have not already uploaded appropriate files and instructions in your readme via ScholarOne Manuscripts, you must inform the production editor of your intention immediately.

3. Correction of proofs:

Our publishing partners, Wiley-Blackwell, will do all they can to publish your paper online within 30 working days of receiving it. This tight production schedule means that, once the .pdf page proofs are ready, we depend on your returning corrected proofs promptly. So, if you are likely to be away during the next eight weeks, please inform the production editors (gji@wiley.com) of the dates and whether/how you may be contacted.

4. Proofs and Offprints:

The typesetters will send you an e-mail with a link to PDF proof of your article. If you are unable to receive proofs in this way please contact the Production Editors (gji@wiley.com) immediately.
GJI no longer provides free offprints, but a .pdf file will be sent to you on publication and you may use this to generate copies for your own use. High quality offprints may be purchased from the publishers at rates given in the e-mail that accompanies proofs.

Finally, on behalf of the Editors and staff of Geophysical Journal International, I thank you for offering us this opportunity to present the valuable results of your research. I trust that you have found the editorial process at GJI fair and efficient. If you have any feedback on that process, my colleagues and I will be pleased to hear it; please address your comments to me, and I will make sure that they are brought to the attention of the relevant member of our team.

We look forward to receiving your further submissions.

Regards,

Mrs. Valerie Dennis
Geophysical Journal International

----- Τέλος προωθημένου μηνύματος -----

--
Skarlatoudis Andreas
Dr. Seismologist,
Geophysical Laboratory,
University of Thessaloniki,
PO Box 352-1, GR-54124,
Thessaloniki, GREECE
Email: askarlat@geo.auth.gr
http:\\seismology.geo.auth.gr\~askar
Tel.: + 30 2310991406
Fax: + 30 2310991403

Local site-effects for the city of Thessaloniki (N. Greece) using a 3D Finite-Difference method: A case of complex dependence on source and model parameters.

A.A. Skarlatoudis[1], C.B. Papazachos[1], N.Theodoulidis[2], J. Kristek[3] and P. Moczo[3]

[1]*Department of Geology, University of Thessaloniki, Thessaloniki-Greece, askarlat@geo.auth.gr, kpapaza@geo.auth.gr*
[2]*ITSAK, Thessaloniki, ntheo@itsak.gr*
[3]*Department of Astronomy, Physics of the Earth and Meteorology, Comenius University, Bratislava, Slovak Republic, kristek@fmph.uniba.sk, moczo@fmph.uniba.sk*

Key words: Earthquake ground motion, site effects, wave propagation

ABSTRACT

The site effects of seismic motion in the metropolitan area of the city of Thessaloniki (Northern Greece) are investigated using a 3D finite-difference modeling approach. Three different seismic scenarios are assumed with two different focal mechanisms for each one. Standard spectral ratios (SSR) are calculated from 3D synthetics and compared with the ratios from the recorded motion, as well as ratios obtained from 1D and 2D modeling by other researchers. The average SSR curves from the six scenarios are in good agreement with the empirical ones, while the SSR results from 3D modeling are different from those from 1D modeling, exhibiting higher fundamental frequencies and larger amplification amplitudes, in much better agreement with observed SSR ratios. Comparisons of Fourier amplitude spectra obtained for various scenarios for the broader area of Thessaloniki show considerable dependence of the site

effects on the source properties (position, depth and fault-plane solution), as well as on the local structure.

1. INTRODUCTION

The city of Thessaloniki (Northern Greece) is located in the Axios-Vardar geological zone, which is adjacent to the Servomacedonian massif, one of the most seismotectonically active regions in Europe (Papazachos et al., 1983) (Figure 1). The seismotectonic setting of the broader area (Servomacedonian massif) is characterized mostly by normal faults with an E-W strike due to the extensive stress field, with a more or less N-S direction, as well as secondary, mainly SE–NW, striking faults (Vamvakaris et al., 2006).

Figure (2a) shows a general overview of the geological structure of the broader study area. Thessaloniki with its suburbs lies across the Thermaikos gulf and is situated on three main large-scale geological formations, oriented in an NW-SE direction, following the well known local Alpine trending of continental-type basins and grabens in this area. The deepest bedrock formation consists of gneiss, epigneiss and green schists, with outcroping manifestation at the N-NE borders of the urban area (dark grey areas in Figures 2a and 2b). These crystalline rocks constitute the bedrock basement, with a depth >400m near the coastline, while its depth is continuously increasing towards the centre of the Thermaikos gulf, where the Neogene sediments exceed the thickness of 2500m (fig. 2a).

Above this basement, the basin has been filled by sedimentary deposits, mainly of the Neogene and Quaternary period (medium and light grey areas in Figure 2b, respectively). These geological formations are dominated by the local red silty clay

series, which cover the bedrock basement beneath the city. Finally, the topmost surface layer consists mainly of recent deposits of Holocene clays, sands and pebbles.

The city has suffered large earthquakes throughout its history (Figure 1) and many of them caused significant damage and human losses (Papazachos and Papazachou, 2002). Thessaloniki was the first big modern city in Greece which was hit by a destructive earthquake (20 June 1978, **M**6.5), attracting several researchers to perform microzonation studies, as well as to quantify site effects and predict structural behavior during strong earthquakes (e.g., Sherif, 1973; Kobayashi, 1974; Leventakis and Roussopoulos, 1974; Pitilakis et al., 1982; Tsotsos and Zissis-Tegos, 1986; Chávez-García et al., 1990; Lachet et al., 1996; Panou et al., 2005; Triantafyllidis et al., 1998, 1999, 2004a,b; Raptakis et al., 1998, 2004a,b).

The first effort that led to the construction of a detailed 3D geophysical/geotechnical model for the sedimentary formations and bedrock geometry of the city of Thessaloniki (model AN01 hereinafter) was performed by Anastasiadis et al. (2001), who studied the 1D geometry and the dynamic properties of major soil formations of the metropolitan area of Thessaloniki using a large number of borehole data and laboratory measurements. The second major effort was conducted by Apostolidis et al. (2004a, b) (model AP04 hereinafter), who performed array ambient noise measurements for 16 sites in the broader area of Thessaloniki using the SPAC technique. The 1D V_s-profiles determined from the inversion of noise dispersion curves for these sites together with the available geotechnical data (mainly from the AN01 model) were used to derive a revised 3-dimensional geophysical model for the study area.

In the present study the finite-difference (FD) method was used to numerically simulate the site response for 11 selected sites of the metropolitan area of Thessaloniki for which earthquake recordings were also available. Theoretical standard spectral ratios

are compared with those obtained from the recorded motions, while spectral ratios (SSR) and Fourier amplitude spectra are used to evaluate the variability of ground motion due to 3D soil response as well as different seismic excitation. As a result, the study does not include any time-domain comparisons but focuses on the validation of the available models in the frequency domain using the available empirical transfer functions for selected sites, in order to quantify the effect of various factors (3D model and its uncertainties, source location, focal mechanisms, etc.) in the final FD synthetics.

2. GEOLOGICAL MODEL

For the model selection, preliminary tests were initially performed for the more recent AP04 model. However, this model was based in a "reverse" approach, where after estimating the V_P and V_S depth variation for the sites where ambient noise measurements were performed, soil formations were determined for the whole study area on the basis of arbitrary V_S velocity intervals. This approach resulted in the introduction of "artificial" model layers (corresponding to specific V_S-velocity intervals) and not to layers that correspond to real geological sedimentary formations, which are better described by the relatively older available model (AN01).

In order to test the effect of this model generation approach on the performance of the AP04 model for FD simulations, a large number of synthetics was computed for the 11 selected sites. Comparisons with empirical transfer functions for most of the sites studied showed a relatively poor performance. This behavior is probably due to the specific velocity averaging and grouping adopted in the AP04 model, hence results for this model were not further examined and only the AN01 model was employed in the present study.

Since the AN01 model covers a part of the metropolitan area of Thessaloniki (fig. 2b), it was extended within the dashed-line area shown in figure (2b) using the general geometry (but not the corresponding grouped velocity values) of the main formations, as provided by the AP04 model (the original coverage of the AN01 and AP04 models is also shown in Figure 2b). This extrapolation mainly concerns areas for which information on the geometry and properties of geological formations was not available for the AN01 model (mainly the northwestern and southeastern part of the model, see Fig. 2b).

For the northeastern part of the model the dominating formation is the bedrock (mainly gneiss), with surface manifestation throughout the largest part of this area (Figure 2b). The AN01 model was also extrapolated towards this direction, adopting the presence of the bedrock formation for the whole NE area of the computational model. Furthermore, for the southwestern part of the model (sea area), where the bedrock depth attains large values and the total sedimentary cover becomes very thick, all layers were arbitrarily extended and thickened. The typical structure of the model formations along a cross-section connecting two of the sites studied (LEP-OBS) with a NE-SW direction and located in the center of the model is also shown in Figure 2b, and clearly verifies the gradual sediment thickening in this direction.. Despite the fact that accurate information for the sea area does not exist, larger scale studies have identified the continuous thickening of Cenozoic sedimentary formations towards the central part of the Thermaikos gulf, several tens of kilometers to the southwest of the city of Thessaloniki (Lalechos and Savoyat, 1979; Roussos, 1994). The continuous thickening of the sedimentary formations towards the W-SW direction is clearly delineated by the Neogene sediments thickness lines from Lalechos and Savoyat (1979) presented in Figure 2a. Taking this into account, the proposed extrapolation approach should have practically no

impact on the modeling results, as in all examined scenarios in the present study the earthquakes were located to the North, Northeast and East of Thessaloniki, where most of the large events of the high seismicity Servomacedonian massif occur (Figure 1). Therefore, seismic waves do not propagate in this SW part of the model before reaching the city of Thessaloniki and significant back-scattering and reflecting energy is not expected from the sea area due to the general gradual increase of the sedimentary layer thickness and the associated bedrock depth. Figure 3 shows the depth variations of the different soil formations of the modified AN01 model, covering an area of 9 x 12 km^2, after the procedure previously described.

3. NUMERICAL-SIMULATION METHOD

For numerical simulations an explicit 3D 4th-order velocity-stress finite-difference scheme was used. The scheme solves the equation of motion and Hooke's law for viscoelastic medium with rheology of the generalized Maxwell body,

$$\rho \dot{v}_i = \sigma_{ij,j} + f_i \tag{1}$$

and

$$\begin{aligned} \dot{\sigma}_{ij} &= \kappa \dot{\varepsilon}_{kk}\delta_{ij} + 2\mu\left(\dot{\varepsilon}_{ij} - \tfrac{1}{3}\dot{\varepsilon}_{kk}\delta_{ij}\right) \\ &\quad - \sum_{l}^{4}\left[\kappa Y_l^{\kappa}\xi_l^{kk}\delta_{ij} + 2\mu Y_l^{\mu}\left(\xi_l^{ij} - \tfrac{1}{3}\xi_l^{kk}\delta_{ij}\right)\right], \end{aligned} \tag{2}$$

$$\dot{\xi}_l^{ij} + \omega_l \xi_l^{ij} = \omega_l \dot{\varepsilon}_{ij} \quad ; \quad l = 1,...,4 \,. \tag{3}$$

Let (x_1, x_2, x_3) be Cartesian coordinates. Then $\rho(x_i)$; $i \in \{1,2,3\}$, is density, $\kappa(x_i)$ and $\mu(x_i)$ are unrelaxed (elastic) bulk and shear moduli, $Y_l^{\kappa}(x_i, \omega_l)$ and $Y_l^{\mu}(x_i, \omega_l)$ anelastic

coefficients, ω_l $l-$th angular relaxation frequency, $\vec{v}(x_i,t)$ particle-velocity vector, t time, $\vec{f}(x_i,t)$ body force per unit volume, $\sigma_{ij}(x_k,t)$ and $\varepsilon_{ij}(x_k,t)$; $i,j,k\in\{1,2,3\}$ stress and strain tensors, $\xi_l^{ij}(x_k,t;\omega_l)$ material-independent anelastic functions. Summation convention does not apply to index l. The anelastic coefficients are obtained from

$$\begin{aligned} Y_l^{\kappa} &= \left(\alpha^2 Y_l^{\alpha} - \tfrac{4}{3}\beta^2 Y_l^{\beta}\right) \Big/ \left(\alpha^2 - \tfrac{4}{3}\beta^2\right), \\ Y_l^{\mu} &= Y_l^{\beta} \quad ; l=1,...,4 \end{aligned} \tag{4}$$

where α and β are elastic (corresponding to the unrelaxed moduli) P- and S- wave velocities, and anelastic coefficients $Y_l^{\alpha}(\omega_l)$ and $Y_l^{\beta}(\omega_l)$ are obtained from the desired or measured quality factor values at frequencies $\tilde{\omega}_k$

$$Q_{\nu}^{-1}\left(\tilde{\omega}_k\right) = \sum_{l=1}^{n} \frac{\omega_l\,\tilde{\omega}_k + \omega_l^2\,Q_{\nu}^{-1}\left(\tilde{\omega}_k\right)}{\omega_l^2 + \tilde{\omega}_k{}^2}\, Y_l^{\nu}(\omega_l) \quad ; k=1,...,7\,, \quad \nu\in\{\alpha,\beta\}\,. \tag{5}$$

The FD scheme sufficiently accurately accounts for the geometry of the material interfaces. The schemes for solving the equation of motion and time derivative of Hooke's law have the same structure as standard 4th-order velocity staggered-grid schemes. The accuracy of the scheme with respect to the material interfaces is due to the definition of the effective material grid parameters. The effective grid density for a corresponding particle velocity component is evaluated as an integral volume arithmetic average of density inside a grid cell centered at the grid position of the corresponding

particle velocity component; for example density at the grid position $I,\ \mathrm{J}+1/2,\ \mathrm{K}+1/2$ is defined by

$$\rho^{A}_{I,\ \mathrm{J}+1/2,\ \mathrm{K}+1/2} = \frac{1}{h^3}\int_{x_{I-1/2}}^{x_{I+1/2}}\int_{y_J}^{y_{J+1}}\int_{z_K}^{z_{K+1}} \rho\ \mathrm{d}x\ \mathrm{d}y\ \mathrm{d}z\,. \tag{6}$$

The effective grid unrelaxed bulk and shear moduli are evaluated as integral volume harmonic averages of moduli in respective grid cells, centered at grid positions of the stress-tensor components; for example

$$\kappa^{H}_{I+1/2,\ \mathrm{J}+1/2,\ \mathrm{K}+1/2} = \left[\frac{1}{h^3}\int_{x_I}^{x_{I+1}}\int_{y_J}^{y_{J+1}}\int_{z_K}^{z_{K+1}} \frac{1}{\kappa}\ \mathrm{d}x\ \mathrm{d}y\ \mathrm{d}z\right]^{-1}. \tag{7}$$

The integrals are evaluated numerically and the grid cell can contain a material discontinuity. The material parameterization enables the FD scheme to sense the true position of the material interfaces, even within a grid cell. The anelastic coefficients Y_l^{κ} and Y_l^{μ} are determined as follows: An average viscoelastic modulus in the frequency domain is numerically determined for a cell as an integral harmonic average. A corresponding quality factor is then determined from the averaged viscoelastic modulus at specified frequencies. Equations (5) for the bulk and shear moduli are then used to determine average anelastic functions. A coarse spatial distribution of the anelastic functions is applied in order to reduce the memory requirements. For more on the scheme for interior grid points and material parameterization see Moczo et al. (2002) and Kristek

and Moczo (2003). For a comprehensive exposition see monograph by Moczo et al. (2007).

Adjusted 4^{th}-order accurate finite-difference approximations are applied at the planar free surface (Kristek et al., 2002). The unsplit PML formulation is used to prevent spurious reflections from the boundaries of the grid (Skarlatoudis et al., 2006; Kristek et al., 2009a).

It is advantageous to cover surface sediments with lower seismic wave velocities by a fine spatial grid and underlying stiffer bedrock with larger velocities by a coarser spatial grid: the number of grid points and consequently the computer memory and time requirements are significantly reduced compared to the uniform grid. In order to make such a combined (or discontinuous) spatial grid efficient, the ratio of the size of the spatial grid spacing in the coarser grid and that in the finer grid should correspond to the ratio of the shear-wave velocities in the stiffer bedrock and softer sediments. Moczo et al. (2007) and Kristek et al. (2009b) present a discontinuous spatial grid that allows choosing the ratio (an odd number) of the spatial grid spacings in the coarser and finer grids.

4. COMPUTATIONAL MODEL

The true model geometry of the material interfaces as well as the smooth material heterogeneity inside the sedimentary body are accounted for in the evaluation of the effective material elastic and anelastic grid parameters using relations (4), (5), (6) and (7) and the approach described therein. As previously noted the scheme using the integral volume harmonic averages of the moduli and integral volume arithmetic average of density, evaluated for each cell centered at a relevant grid position, is capable to sense the true position of the material interfaces within the grid cell.

The constant $Q(\omega)$ law is simulated using the rheology of the generalized Maxwell body. The so-called coarse grid graining is applied in the spatial discretization of the anelastic coefficients and functions. Since for the existing models Q_α values were not available, they were estimated using the relation

$$\frac{1}{Q_\alpha} = \frac{4}{3}\left(\frac{\beta^2}{\alpha^2}\right)\frac{1}{Q_\beta} \ . \tag{8}$$

Values of the material parameters in each formation in the adopted model, Figure 3, are listed in Table 1.

For all computations, the adopted approach requires that the computational model must include the hypocenters of the earthquakes to be modeled, thus, the modified AN01 geophysical/geotechnical model (Figure 3) should be sufficiently large to meet this condition. As previously mentioned, the modeled earthquake hypocenters in the present study were located to the North, Northeast and East of Thessaloniki (see also Figure 4). Therefore, the northern and eastern parts of the modified AN01 geophysical/geotechnical model (Figure 3) were extrapolated towards these directions. Due to the lack of detailed information on the 3D geometry and material parameters of the formations in these areas, the modified AN01 model was arbitrarily expanded by adopting the formation geometry of the model's Northern and Eastern edge and the dominant local Alpine trend of the sedimentary and bedrock formations in the area (NW-SE), also seen in the general geological outline and morphology presented in Figures 2a and 4. In other words, the Northern and Eastern model vertical cross-sections were replicated and appropriately shifted in order to obtain a bedrock-sediment surface geometry that matches the surface

geology (bedrock-sediment contact) and geomorphology. The final computational model dimensions after this extrapolation are shown in Table 2 and its spatial extent is seen in Figure 4. The framed areas correspond to the modified AN01 model.

It should be noted that this extrapolation approach, despite being only roughly realistic, is not expected to significantly affect the obtained results, since seismic waves generated at typical focal depths (5-10 km) and propagating towards Thessaloniki area (southwestern part of the model) are not generally influenced by e.g. the presence of a small isolated surface sedimentary basin on top of the bedrock formation, just above the hypocentral area. Furthermore, the geometry of the artificially generated southeastern and northwestern sections of the enlarged model suggests that no waves travelling in these model parts will influence the main characteristics of the wave propagation in the broader Thessaloniki metropolitan area (southwestern part of the model of Figure 4). This assumption was verified by both qualitative and quantitative tests (e.g. adopting different model enlargement strategies).

Given the size of the desired computational model and S-wave velocities in the model, the size of the spatial grid spacing was chosen to be 15m in the finer grid. Assuming 6 grid spacings per minimum S-wavelength as sufficient spatial sampling, the maximum frequency up to which the simulation can be considered as sufficiently accurate is 2Hz. Given the maximum S-wave velocity in the model, 3400 m/s and the smallest horizontal dimension of the model, 16200 m, the simulation should only be considered for frequencies larger than 0.2 Hz. The time step for the FD computations was estimated using the equation:

$$\Delta t \le \frac{6}{7\sqrt{3}} R, \quad R = \frac{\Delta h_{\min}}{V_{p_{\max}}} \tag{9}$$

[11]

where $\Delta h_{\min}$ is the minimum grid step used in the computation and $V_{P\max}$ is the maximum P wave velocity of the computational model (Moczo et al., 2000). The time step estimated from equation (9) for the simulations is 0.0012 s and the computational parameters are summarized in Table 2.

Six earthquake scenarios were considered, with two different focal mechanisms for each of three hypocentral positions examined. The computational model together with the epicenters and focal mechanisms of the earthquake scenarios are shown in Figure 4. Geographical coordinates and focal parameters are summarized in Table 3. The same moment magnitude (**M**5.1) and the hypocentral depth (5Km) was assumed for each of the six earthquakes. One additional numerical simulation was performed for a hypocentral depth of 10 km for the epicentral position 1.

A double-couple point source was assumed for each scenario. For the source-time function, representing particle velocity, a Gabor signal was assumed of the form,

$$s(t) = \exp\left\{-\left[\omega\left(t-t_s\right)/\gamma\right]^2\right\}\cos\left[\omega\left(t-t_s\right)+\theta\right]. \qquad (10)$$

Here, $\omega = 2\pi f_p$, $t \in [0, 2t_s]$, f_{p} is the dominant frequency, γ controls the width of the signal, and θ is the phase shift. The source-time function parameters are given in Table 4, while the signal and its Fourier spectrum are shown in Figure 5.

For the receivers 11 grid positions were chosen, corresponding to sites for which seismic records were available from a local network of seismographs and accelerographs which operated in the broader area of Thessaloniki during four months (November 1993 - February 1994, Lachet et al., 1996). Figure 4 (left panel) shows the receiver positions and

Table 5 lists code names and coordinates. Moreover, a dense grid of receiver positions was also considered in order to study the spatial variation of the simulated motion in the metropolitan area of Thessaloniki (Figure 4, right panel).

5. EVALUATION OF SITE RESPONSE

The accuracy of the model used in the computations is a critical issue that affects the accuracy and credibility of the resulted waveforms; therefore it was necessary to further evaluate its impact on the determined site response. For this reason, two different approaches for the model extension procedure (described in the previous paragraph) have been implemented and the corresponding synthetic results have been produced. The first approach involves the extension of the model to the North, assuming a dominant N-S direction for the bedrock-sediments interface, i.e. practically replicating towards the North the northernmost E-W trending slice of the basic model of figure 2b. The second approach corresponds to the procedure described in the previous paragraph, which involves the same extension adopting the dominant NW-SE direction of the bedrock-sediments boundary, also shown in Figure 2a. Comparisons for the two models expansion procedures were performed for two of the sites where empirical SSR were available, namely site AMP which is the closest to the NW part of the model which was expanded and site AGO located in the center of the model. In Figure 6 the results of this comparison both in the time and frequency domain for scenario 1a are presented, showing that the two different model expansion approaches have, practically, no impact on the synthetic waveforms. Moreover, the wave propagation characteristics that are presented in a video file compiled from the time snapshots of the N-S component for the model with the NW-SE extension of the bedrock (included as an electronic supplement)

also verify the previous conclusions, as almost no back-scattering from this expanded part of the model towards the main model body (including the 11 sites) is observed.

The evaluation of site response was performed using the SSR approach (Borcherdt, 1970). The geometric mean of smoothed Fourier Amplitude Spectra (FAS) of the horizontal components for all six seismic scenarios was calculated and used for obtaining the synthetic SSR curves. Station OBS, which is located on bedrock, was used as a reference site, in accordance with previous studies employing either real or synthetic recordings for the city of Thessaloniki. The synthetic SSR curves derived in the present study have been compared with the empirical SSR curves from Lachet et al. (1996) (based on velocity recordings) and from Triantafyllidis et al. (2004b) (based on accelerograms).

All empirical and synthetic FAS were smoothed with the Konno and Ohmachi (1998) technique (smoothing parameter b=20), with the exception of original synthetic and empirical results from Triantafyllidis et al. (2004b), where a moving window of 0.5Hz with a 50% overlap was applied by the authors. In Figure 7 comparisons between synthetic and empirical SSR curves are shown. The thick black curve corresponds to the average SSR curve from all six scenarios, while its standard deviation is shown by the dashed line. Empirical SSR curves by Lachet et al. (1996) (light blue) and Triantafyllidis et al. (2004a) (green) are also presented. The maximum frequency (f_{max}) up to which FD calculations in the present study should be sufficiently accurate is denoted with a red line.

Comparisons between the empirical (Lachet et al, 1996; Triantafyllidis et al., 2004a) and the average synthetic SSR curves computed in the present study (Figure 7) are in a good agreement for the majority of the studied sites - both in terms of amplitudes and fundamental frequencies. Larger differences between the predicted and empirical SSR can be seen at sites where the model has been extended (e.g sites AMP, KAL, see

Figure 2b). However, given the geophysical/geotechnical model inherent uncertainties, the numerical predictions can be characterized as satisfactory. Furthermore, it should be pointed out that the presented empirical SSR curves have been calculated from recordings of earthquakes at various epicentral distances, different magnitudes and focal mechanisms. On the other hand the SSR curves computed in the present study from the FD simulations have been computed based on a limited number of earthquake scenarios and focal mechanisms, magnitudes and epicentral distances.

Results have been also compared with theoretical SSR curves from 1D methods such as modal summation (Panza, 1985; Panza and Suhadolc, 1987) and reflectivity method (Kennett, 1983), as applied by Triantafyllidis et al. (2004a) and Raptakis et al. (2004a), respectively. Comparisons with 2D theoretical modeling were performed using results from the hybrid (Fah, 1992) and FD method (Moczo, 1989; Moczo and Bard, 1993), as applied by Triantafyllidis et al. (2004a) and Raptakis et al. (2004b), respectively, for the broader area of Thessaloniki. The theoretical SSR curves from the 1D and 2D numerical modeling are also shown in Figure 7.

The results presented in Figure 7 clearly demonstrate that the average 3D model synthetic SSR curves estimated in the present study exhibit a superior performance with respect to the 1D and 2D numerical modeling, regarding both the fundamental frequency and amplification levels derived from the observed SSR curves. It could be argued that the observed discrepancies, which are occasionally large (e.g. sites OTE, ROT) can be justified, to a certain extent, by the fact that 1D and 2D synthetics computed by the various researchers, were not based exactly on the same geophysical-geotechnical model. Therefore, even minor differences in the input model configuration used in the various studies may become important, especially for sites that are situated in the extrapolated areas of the AN01 model.

In order to examine this issue, additional synthetics (1D synthetics hereinafter) have been computed with the program Axitra [program by O. Coutant based on Discrete Wavenumber Method (DWN) by Bouchon, 1981] for each site using the local 1D structure extracted from the constructed 3D model. For the simulation a point-source (3D wavefield), with the same properties as the one used in FD simulations, has been used in order to account only for the 1D structure effects in the SSR comparisons. Therefore the term "1D synthetics" actually refers to synthetics for 1D structure and not to synthetics for 1D structure and 1D wavefield. Comparisons between average 3D (black solid) and 1D (black dashed) synthetic SSR curves are shown for the six scenarios in Figure 8a, where the observed SSR curves (grey curves) by Lachet et al. (1996) are also superimposed. In these figures, similar behavior as the one described in Figure 7 can be identified for the majority of the studied sites, with the 3D SSR curves exhibiting a much better agreement with the observed SSR results, regarding both the fundamental frequency and SSR amplitude and shape characteristics.

This agreement is further quantified in Figure 8b, where the empirical fundamental frequency and the corresponding SSR amplification from Lachet et al. (1996) is plotted against the theoretical results from both 1D and 3D simulations. In almost all cases the results from the 3D modeling are much better correlated with the observed (empirical) SSR frequencies and amplitudes. Given that the local geophysical model employed and source properties are the same, the differences between 1D and 3D results reflect the lower efficiency of the 1D simulations in describing the site response for the examined sites. An exception is the amplification amplitude for station AGO, which is the site with the highest fundamental frequency (small sedimentary cover thickness). This discrepancy is probably due to the fact that the employed FD modeling should be sufficiently accurate up to 2Hz and practically of acceptable accuracy up to ~4-4.5Hz, as is evident from the

variability of the individual SSR results from the different scenarios later presented (Figs. 9 and 10). Therefore, the frequency and especially the theoretical SSR amplitudes for station AGO (fundamental frequency from 3D model ~5Hz) should be considered as inaccurate.

As was pointed out by other researchers (e.g. Semblat et al., 2005; Makra et al., 2002) who compared results from 1D and 2D analysis, higher-order simulations tend to predict higher amplifications, which are also shifted towards higher resonant frequencies when compared to those predicted from lower-order simulations. This effect is attributed to the contribution of the models' lateral heterogeneities in the amplification of ground motions. In other words, the effect of lateral heterogeneity of the model on propagation of surface waves, results in more pronounced amplification shifted towards higher frequencies.

The previously described pattern is also observed in the 3D synthetics calculated in the present study (see Figure 8a and left panel of Figure 8b). This is more evident in Figure 9a, where the relative increase of the fundamental frequency estimated from FD simulations (F3D) with respect to the one from the DWN simulations (F1D) is plotted against F1D. A clear, almost linear, increase of the relative frequency shift with respect to F1D can be observed for sites with F1D spanning the range 0.5-2.5Hz (F3D 0.5-3.5Hz), with the exception of site AGO, for which the relative change can be considered as inaccurate, as previously explained. The three sites (OTE, LAB and ROT) exhibiting the higher relative values of frequency shifting are located on intermediate thickness soil formations (F1D ~1.5-2.5Hz), verifying the correlation of the frequency shifting with the local site's structure (higher frequency shifting for higher F1D).

In Figure 9b the relative increase of the 3D SSR fundamental amplitude (AMP3D), with respect to the one of 1D simulations (AMP1D), is plotted against AMP1D. The most

prominent feature is the high relative values of 3D to 1D amplifications observed in the coastal zone, as defined by sites TYF, LEP and possibly POL (see also Figure 4). This zone is characterized by relatively thick soil formations and high absolute values of amplifications. Most of the other sites studied do not exhibit noticeable relative SSR amplification changes (maximum variation of ~±20%).

It should be pointed out that for some sites (e.g. LEP and TYF), located in the area of the Thessaloniki's city center, a good agreement, is found between results from 2D and 3D numerical modeling. It has to be pointed out that this agreement only concerns the predicted fundamental frequency for the examined sites and not the amplitude or the general shape characteristics of the corresponding SSR curves. This observation supports the findings of other researchers (e.g. Panou, 2005) who showed the dominant control of the 2-dimensional geometry of soil formations on the site response characteristics. Nevertheless, the majority of comparisons between results from 1D, 2D and 3D numerical modeling confirm the significant impact of the 3D model structure on the detailed characteristics of seismic motion for the broader Thessaloniki area.

6. DEPENDENCE OF SITE RESPONSE ON SOURCE AND MODEL GEOMETRY

The variability of the mean SSR depicted by the corresponding standard deviation (Figure 7 - black dashed lines) is a consequence of the differences between the individual SSR ratios of the six scenarios studied. These differences are found not only among scenarios with different hypocenter locations, but also between scenarios with the same hypocenter location and different focal mechanisms. The influence of the focal mechanism on the local amplification of the seismic motion has been identified also by

other researchers (e.g. Field, 1996; Riepl et al., 1998) as a factor that could significantly bias the estimated site response. An example is given in Figure 10, where for four selected sites the SSR curves from six scenarios are shown (red, green and blue dashed and solid lines), together with the mean curve (black line) and empirical SSR curves (light blue) from Lachet et al. (1996). In some cases, e.g. for site TYF, strong differences are observed between scenarios 2 (blue solid and dashed curves, which correspond to different focal mechanisms) both in terms of amplitude and fundamental frequency, in the frequency range 0.2Hz-4Hz. For site POL these differences are found in both scenarios 1 (red curves) and 2 (blue curves) for the same frequency window. On the other hand, there are sites, e.g. LAB and ROT, where all six scenarios produce quite similar results, with little variability.

Similar conclusions are drawn when the dependence of local site response on the focal depth of the earthquake is examined. For this reason scenarios 1a and 1b have been computed using a focal depth of 10Km and compared with the ones computed for a depth of 5km. Comparisons are shown in Figure 11, where the SSR curves for 5km and 10 km are denoted with the red and green colors, respectively. Average SSR curve (black) from six scenarios and empirical SSR curves by Lachet et al. (1996) (light blue) are also shown. For the majority of examined sites, comparisons show that local site effects also depend on the focal depth of the earthquake, but not as significantly as on the focal mechanism. Again, there are sites that exhibit practically the same SSR pattern, independently of the focal depth of the earthquake (e.g AGO, LAB, ROT), while sites with thicker soil formations (e.g. KAL, LEP, TYF) show differences, mostly in the predicted amplification levels (in most cases lower amplifications for the larger focal depth scenarios – green curves). The previous results imply that a unified and unique local site response cannot be determined for different seismic excitations, at least not for

all sites studied, since a strong dependence of local site response on the source properties (focal mechanism, depth) and location is observed.

Nevertheless, except for the effect of the focal parameters, the geophysical model's structure itself remains the dominant factor controlling the local site response. In order to demonstrate the impact of the AN01 model on seismic motion for the broader area of Thessaloniki, the Fourier Amplitude Spectra (FAS) spatial distribution was examined. FAS of ground acceleration have been computed for the dense grid of receivers (Figure 4b), for all six scenarios. In order to minimize source (radiation pattern) and geometric spreading effects and enhance the effect of the 3D geometry of soil formations, FAS were calculated for the AN01 geophysical model (FAS3D) and for the corresponding bedrock 1D model (FAS1D). Therefore the (FAS3D)/(FAS1D) ratio mainly reflects the spectral amplification due to the 3D structure of the geophysical model, with source and path effects partly eliminated.

In Figure 12 the spatial variation of the examined ratios for the three components of ground motion is shown for the six scenarios studied and for the frequency of 1Hz. The area covered in Figure 12 corresponds to the area of the computational model. The N-S component exhibits the lowest spectral relative amplification values (FAS3D/FAS1D) for all six scenarios. For scenario 2a, though, for the north-western parts of the model the peak values predicted are much higher (~9). For the E-W component the highest values are predicted for scenarios 1a and 3a for the south-eastern part of the model. Maximum amplification levels predicted are as high as 14-16 for scenario 1a and ~10 for scenario 3a. For the remaining cases relatively high values of amplification (5-6) are found only for smaller parts of the model, mostly in the center of the metropolitan area of Thessaloniki. Vertical components exhibit, as expected, much lower amplification amplitudes than the horizontal ones. Nevertheless, the largest vertical amplification

amplitudes are observed for scenarios (1) (up to ~9), mostly in the central part of the coastal zone, where thicker sediments dominate the local structure. It has to be stressed that FAS spatial distribution has been studied for a larger set of periods, not shown here for practical reasons and a similar spatial distribution pattern as the one described in Figure 12 has been observed.

7. DISCUSSION-CONCLUSIONS

In the present study the site response for selected sites in the metropolitan area of Thessaloniki (Northern Greece) has been evaluated using the 3D finite-difference modeling. Synthetic waveforms for six seismic scenarios with different source properties (hypocenter and focal mechanism) derived from the well known seismotectonic characteristic of the broader area of Thessaloniki have been computed.

The geophysical-geotechnical 3D model proposed in this study is based on both available 3D models for the broader area of Thessaloniki, namely the results of Anastasiadis et al. (2001) (model AN01) and Apostolidis et al. (2004a, b) (model AP04). These two models do not cover the same area, with the AN01 covering mostly the broader area of the historical center of the city. The computational model used in the FD simulations is based mostly on the extended AN01 model (dynamic properties and layer geometry), as expanded to cover the whole area of interest, using either the AP04 model or assumptions based on surface geology, which are not expected to significantly affect the simulations.

Comparisons have been performed between synthetic and empirical SSR spectral amplification curves. The average synthetic SSR curves from the six scenarios of the 3D FD modeling are in a very good agreement with the empirical ones for the majority of the

studied sites. These comparisons constitute strong evidence about the reliability of the obtained results, since empirical curves represent earthquakes with a much larger spatial variation in comparison to the FD synthetics that were computed for a relatively limited number of seismic scenarios.

Comparisons of the average synthetic 3D SSR curves with SSR curves from 1D and 2D numerical modeling showed that in most of the cases the 3D modeling and its corresponding SSR curves describe much more efficiently the spectral characteristics (in terms of fundamental frequency and site amplification) of the sites studied. Furthermore, the obtained results verify that 3D simulations tend to predict higher amplifications mostly for the thicker sediments of the coastal zone, where high absolute values of SSR amplifications are found. Moreover, an almost linear relative fundamental frequency shift to higher values than those predicted from 1D simulations is observed for thinner sedimentary cover sites (higher 1D fundamental frequencies), with some sites (OTE, LAB and ROT) showing a >50% or larger relative frequency shift. These results are in good agreement (but are also more pronounced) with earlier comparisons between 2D and 1D synthetics.

The relatively large standard deviation of the mean SSR for most examined sites is a direct consequence of the variability among the individual SSR of the six scenarios studied. In addition, similar behavior is shown when the dependence of local site response on the focal depth of the earthquake is examined. These results imply that a single local site response cannot be uniquely determined for different seismic excitations, at least not for all studied sites of the city of Thessaloniki, since a strong dependence of local site response on both focal mechanism and hypocenter location has been observed.

It should be noted, however, that the 3D geophysical-geotechnical model structure still plays a dominant role in forming the local site response. The impact of the employed

AN01 model on seismic motion for the broader area of Thessaloniki is more clearly examined by using the spatial variations of the relative FAS amplifications. The results of the FAS study, together with the aforementioned ones, verify that the variations among scenarios with different hypocenters (scenarios 1, 2 and 3) and different focal mechanisms (scenarios a and b), are a consequence of the dependence of local site response on various parameters (source parameters, location and model structure), for different seismic excitations. This result suggests that, generic or even 1D local site responses should be used with caution when studying soil and structure behavior for specific earthquakes, at least for the Thessaloniki area.

In most of the cases the previous results exhibit the superiority of 3D-FD simulations in comparison with the 1D and 2D ones, in predicting SSR fundamental frequencies and amplification levels for several sites in the area of Thessaloniki. However, in future studies, assuming that the quality and the number of the available empirical data would be sufficiently adequate, the non-linear behavior of soil formations should be also taken into account in simulations for the realistic estimation of 3D-SSR, in cases of strong seismic excitation.

Acknowledgements

We would like to thank Dr Zhou Bing and an anonymous reviewer for their comments and suggestions which helped to improve the present work. This work has been partly supported by project PENED-2003 (measure 8.3, action 8.3.4 of the 3rd Community Support Programme) and the Greek-Slovak Cooperation Agreement (EPAN 2004-2006).

References

Anastasiadis A., D. Raptakis and K. Pitilakis, (2001). Thessaloniki's detailed Microzoning: Subsurface structure as basis for site response analysis. *Pure Appl. Geophys.*, **158**, 2597–2633.

Apostolidis P., D. Raptakis and K. Pitilakis, (2004a). The Use Of Microtremors For The Definition Of Soil Properties And Bedrock Depth In An Urban Area. *Proc. of 13th World Conference On Earthquake Engineering, Vancouver, B.C., Canada.*

Apostolidis P., D. Raptakis, Z. Roumelioti, K. Pitilakis, (2004b). Determination of S-wave velocity structure using microtremors and SPAC method applied in Thessaloniki (Greece). *Soil Dyn. Earthquake Eng.*, **24**, 49–67.

Borcherdt, R.D., (1970). Effects of local geology on ground motion near San Francisco Bay, *Bull. Seism. Soc. Am.*, **60**, 29-61.

Bouchon, M., (1981). A simple method to calculate Green's functions for elastic layered media, *Bull. Seism. Soc. Am.*, **71**, 959-971.

Chávez-García F. J., G. Pedotti, D. Hatzfeld and Pierre-Yves Bard, (1990). An experimental study of site effects near Thessaloniki (northern Greece), *Bull. Seism. Soc. Am.,* **80**, 784-806.

Fäh, D., (1992). A hybrid technique for the estimation of strong ground motion in sedimentary basins, *Ph.D. Thesis*, Nr 9767, Swiss Federal Institute of Technology, Zurich.

Field, E.H., (1996). Spectral amplification in a sediment-filled valley exhibiting clear basin-edge induced waves, *Bull. Seism. Soc. Am.,* **86**, 991-1005.

Kennett, B.L.N., (1983). Seismic Wave Propagation in Stratified Media, *Cambridge University Press*, Cambridge.

Kobayashi H., (1974). Preliminary report on the Microtremor measurements in Thessaloniki, UNPD/SFREM.70.172.

Konno, K., and T. Ohmachi (1998). Ground-motion characteristics estimated from spectral ratio between horizontal and vertical components of microtremor, *Bull. Seismol. Soc. Am.,* **88**, 228-241.

Kristek, J., P. Moczo, and R. J. Archuleta, (2002). Efficient methods to simulate planar free surface in the 3D 4th-order staggered-grid finite-difference schemes, *Studia Geophys. Geod.*, **46**, 355-381.

Kristek, J. and P. Moczo, (2003). Seismic wave propagation in viscoelastic media with material discontinuities – a 3D 4th-order staggered-grid finite-difference modeling, *Bull. Seism. Soc. Am.*, **93**, 2273-2280.

Kristek, J., P. Moczo, and M. Galis, (2009a). A Brief Summary of Some PML Formulations and Discretizations for the Velocity-Stress Equation of Seismic Motion. *Studia Geophys. Geod.*, (in press).

Kristek, J., P. Moczo, and P. Pazak (2009b). Numerical modeling of earthquake motion in Grenoble basin, France, using a 4th-order velocity-stress arbitrary discontinuous staggered-grid FD scheme, in *ESG 2006, Third Intl. Symposium on the Effects of Surface Geology on Seismic Motion*, edited by P.-Y. Bard, et al., Vol. **2**, paper S12, 10 pages, (LCPC Editions, in press), Grenoble.

Lachet C., D. Hatzfeld, P.-Y. Bard, N. Theodulidis, Ch. Papaioannou and A. Savvaidis, (1996). Site effects and microzonation in the city of Thessaloniki (Greece) comparison of different approaches, *Bull. Seism. Soc. Am.*, **86**, 1692-1703.

Lalechos, N. and Savoyat, E., (1979). La sedimentation Neogene dans le Fosse Nord Egeen, *6th Colloqium on the Aegean region*, **2**, 591-603.

Leventakis G. and A. Roussopoulos, (1974). Progress report on Microzoning in Greece by the Greek working group, Athens.

Makra K., D. Raptakis, F.J. Chavez-Garcia, K. Pitilakis, (2002). How Important Is The Detailed Knowledge Of A 2D Soil Structure For Site Response Evaluation?, *12th European Conference on Earthquake Engineering*, 9-13 September, London, UK.

Moczo, P., (1989). Finite-difference technique for SH-waves in 2-D media using irregular grids - application to the seismic response problem, *Geophys. J. Int.*, **99**, 321-329.

Moczo, P. and P.-Y. Bard, (1993). Wave diffraction, amplification and differential motion near strong lateral discontinuities, *Bull. Seism. Soc. Am.*, **83**, 85-106.

Moczo, P., J. Kristek, and L. Halada, (2000). 3D 4th-order staggered-grid finite difference schemes: stability and grid dispersion, *Bull. Seism. Soc. Am.*, **90**, 587-603.

Moczo, P., J. Kristek, V. Vavryčuk, R. J. Archuleta, and L. Halada, (2002). 3D heterogeneous staggered-grid finite-difference modeling of seismic motion with volume harmonic and arithmetic averaging of elastic moduli and densities, *Bull. Seism. Soc. Am.*, **92**, 3042-3066.

Moczo, P., J. Kristek, M. Galis, P. Pazak, and M. Balazovjech, (2007). The finite-difference and finite-element modeling of seismic wave propagation and earthquake motion, *Acta Physica Slovaca*, **57**, 177-406.

Panou A. A., Theodulidis N., Hatzidimitriou P., Stylianidis K., and Papazachos C. B., (2005). Ambient Noise horizontal-to-vertical spectral ratio in estimating site effects and seismic damage distribution in urban environment: The case of Thessaloniki city (Northern Greece), *Soil Dynamics and Earthquake Engineering*, **25**, 261-274.

Panza, G.F., (1985). Synthetic Seismograms: The Rayleigh waves modal summation, *J. Geophys.*, **58**, 125-145.

Panza, G.F. and P. Suhadolc, (1987). Complete Strong Motion Synthetics, In Seismic Strong Motion Synthetics, *Computational Techniques*, **4**, B.A. Bolt (Editor), Orlando, Academic Press, 153-204.

Papazachos B.C., and Papazachou A., (2002). Earthquakes of Greece, Ziti Publications, Thessaloniki, 304pp.

Papazachos, B. C., Tsapanos, T. M. and Panagiotopoulos, D., (1983). The time, magnitude and space distribution of the 1978 Thessaloniki seismic sequence. The Thessaloniki northern Greece earthquake of June 20, 1978 and its seismic sequence. *Technical chamber of Greece, section of central Macedonia*, 117-131, 1983.

Pitilakis K., S. Tsotsos and Th. Hatzigogos, (1982). Study of liquefaction potential in the area of Thessaloniki, *7th Symp. on Earth. Engin.*, Sarita Prakashan, Meerut, India.

Raptakis D., A. Anastasiadis and K. Pitilakis, (1998). Preliminary instrumental and theoretical approach of site effects in Thessaloniki, *11th European Conference on Earthquake Engineering*, Rotterdam, Netherlands.

Raptakis D., K. Makra, A. Anastasiadis and K. Pitilakis, (2004a). Complex site effects in Thessaloniki (Greece): I. Soil structure and comparison of observations with 1D analysis, *Bull. Of Earth. Eng.*, **2**, 271-300.

Raptakis D., K. Makra, A. Anastasiadis and K. Pitilakis, (2004b). Complex site effects in Thessaloniki (Greece): II. 2D SH modeling and engineering insights, *Bull. Of Earth. Eng.*, **2**, 301-327.

Riepl J., P.-Y. Bard, D. Hatzfeld, C. Papaioannou and S. Nechtschein, (1998). Detailed Evaluation of Site-Response Estimation Methods across and along the Sedimentary Valley of Volvi (EURO-SEISTEST), *Bull. Seism. Soc. Am.*, **88**, 488-502.

Roussos, N. (1994). Stratigraphy and paleogeographic evolution of the Paleocenemolassic basins of the North Aegean area, *Bull. Geol. Soc. Greece*, **30**, 275–294.

Semblat J.F., M. Kham, E. Parara, P.Y. Bard, K. Pitilakis, K. Makra, D. Raptakis, (2005). Seismic wave amplification: Basin geometry vs soil layering, *Soil Dynamics and Earthquake Engineering*, **25**, 529-538.

Sherif M.A., (1973). Microzonation of Thessaloniki, using the Sherif-Bostrom (USA) method, prepared for UNDP/UNESCO survey of the seismicity of the Balkan region, Seattle, Washington, USA.

Skarlatoudis A.A., J. Kristek, P. Moczo, C. B. Papazachos, (2006). Implementation of a Non-Splitting Formulation of Perfect Matching Layer in a 3D 4th-order Staggered-grid Velocity-stress Finite-difference Scheme, *1st European Conference on Earthquake Engineering and Seismology*, Geneva, Switzerland.

Tranos M.D., Papadimitriou E.E, and Kilias A.A., (2003). Thessaloniki – Gerakarou Fault Zone (TGFZ): the western extension of the 1978 Thessaloniki earthquake fault (Northern Greece) and seismic hazard assessment, *J. of Struct. Geol.*, **25**, 2109 – 2123.

Triantafyllidis, P., P. M. Hatzidimitriou, P. Suhadolc, N. Theodulidis, and K. Pitilakis, (1998). Comparison Between 1-D and 2-D Site Effects Modelling in Thessaloniki, in "The Effects of Surface Geology on Seismic Motion", **2**, 981-986.

Triantafyllidis, P., P. M. Hatzidimitriou, N. Theodulidis, P. Suhadolc, C. Papazachos, D. Raptakis, and K. Lontzetidis, (1999). Site Effects in the City of Thessaloniki (Greece) Estimated From Acceleration Data and 1-D Local Soil Profiles, *Bull. Seism. Soc. Am.*, **89**, 521-537.

Triantafyllidis P., P. Suhadolc, P.M. Hatzidimitriou, A. Anastasiadis and N. Theodulidis, (2004a). PART I: Theoretical Site Response Estimation for Microzoning Purposes, *Pure Appl. Geophys.*, **161**, 1185-1203.

Triantafyllidis P., P.M. Hatzidimitriou, P. Suhadolc, N. Theodulidis and A. Anastasiadis, (2004b). PART II: Comparison of Theoretical and Experimental Estimations of Site Effects, *Pure Appl. Geophys.*, **161**, 1205-1219.

Tsotsos S. and G. Zissis-Tegos, (1986). Seismic microzonation study of Thessaloniki area and comparison with the observed damage distribution during the June, 1978, earthquake, *Proc. Of the 8th European Conf. on Earth. Engin.*, Lisbon, Portugal.

Vamvakaris D. A., Papazachos C. B., Karagianni E.E., Scordilis E.M., Hatzidimitriou P.M., (2006). Small-scale spatial variation of the stress field in the back-arc Aegean area: Results from the seismotectonic study of the broader area of Mygdonia basin (N. Greece), *Tectonophysics*, **417**, 249–267.

Tables

Table 1. P-wave velocity α, S-wave velocity β, density ρ, P-wave quality factor Q_α and S-wave quality factor Q_β for the 3D AN01 model (Anastasiadis et al. 2001).

Formation	***α (m/s)***	***β (m/s)***	***ρ (gr/cm^3)***	***Q_α***	***Q_β***
A	1050	250	2050	260	15
B	1850	180	2300	1130	25
C	1900	300	2150	510	20
E/F	3000	700	2350	690	50
Bedrock (at free surface)	4500	2000	2600	450	200
Bedrock (1000m)	6000	3400	2600	450	200

Table 2. Computational model parameters

Model dimensions : X=22545 m, Y=16200 m, Z=12105 m
Grid spacing : 15 m in the finer grid (0 – 1170 m), 135 m in the coarser grid
Number of grid cells : (1503 x 1080 x 78) + (167 x 120 x 81) = 128235960
Frequency range : 0.2 – 2.0 Hz
Time step : 0.0012 s
Time window : 20 s
PML zone thickness : 90 grid spacings in the finer grid 10 grid spacings in the coarser grid

Table 3. Focal parameters of the earthquakes used for the computation of synthetic waveforms. All earthquakes have the same moment magnitude (**M**5.1) and focal depth (5Km), except when otherwise specified in the text.

A/A	Lon (E)	Lat (N)	Strike	Dip	Rake
1a	23.0743	40.750	90	55	-70
1b	23.0743	40.750	135	55	-90
2a	23.0743	40.597	90	55	-70
2b	23.0743	40.597	135	55	-90
3a	22.9295	40.750	90	55	-70
3b	22.9295	40.750	135	55	-90

Table 4. Source time function parameters used in the FD computations.

	γ	f_p	θ	t_S
Scenarios 1,2,3	0.25	0.2	$\pi/2$	1.0

Table 5. Code names and coordinates of examined sites, where experimental data were also available for comparison.

A/A	Code name	Lon (E)	Lat (N)
1	AGO	22.9459	40.6374
2	AMP	22.9215	40.6541
3	KAL	22.9485	40.5812
4	LAB	22.9592	40.6285
5	LEP	22.9495	40.6251
6	OBS	22.9628	40.6318
7	OTE	22.9343	40.6398
8	POL	22.9557	40.5949
9	ROT	22.9529	40.6330
10	THE	22.9670	40.6370
11	TYF	22.9530	40.6140

Figures

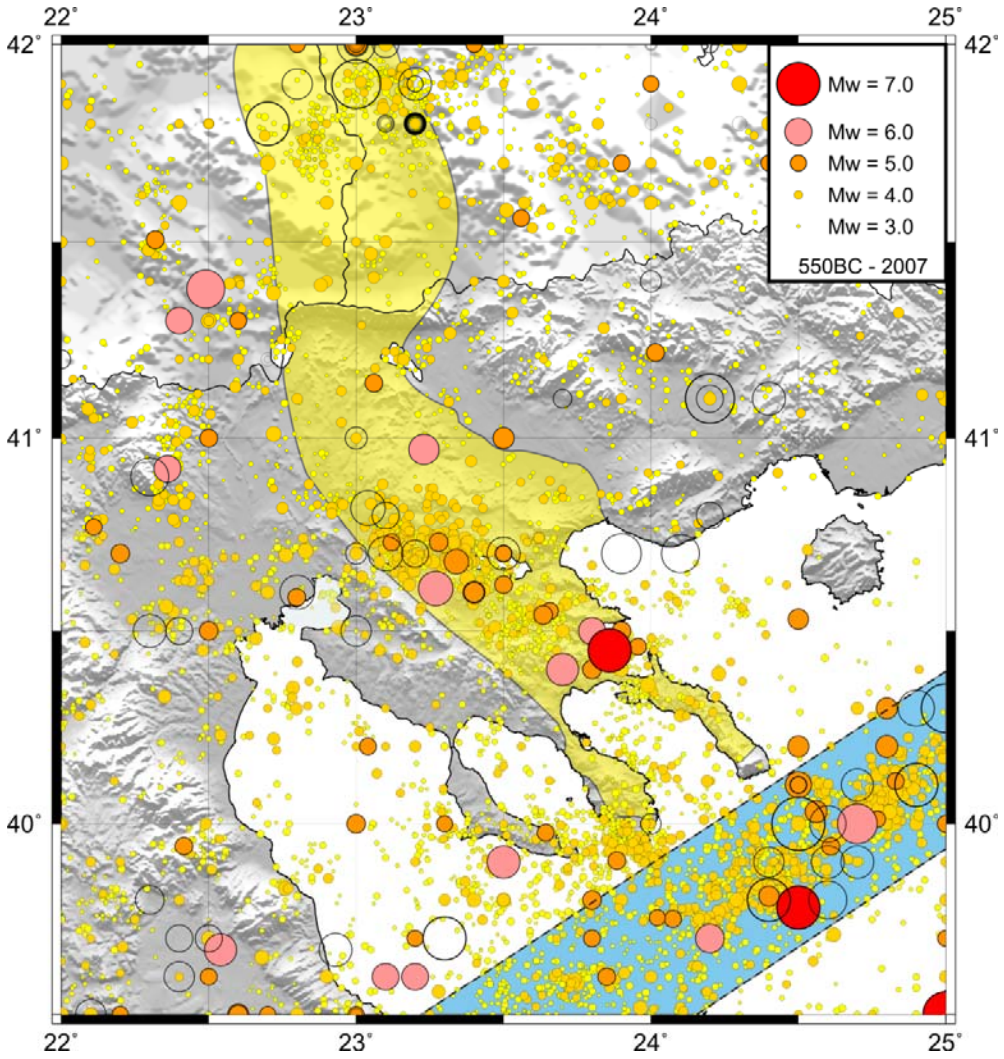

Figure 1. Map of known earthquakes with M≥3.0 which occurred in the broader area of central–northern Greece from the historical times (550 BC) till 2007. Open circles denote epicenters of historical earthquakes (before 1911). Two areas of high seismicity level can be identified, namely the Servomacedonian massif (yellow area) and the North Aegean Trough (blue area).

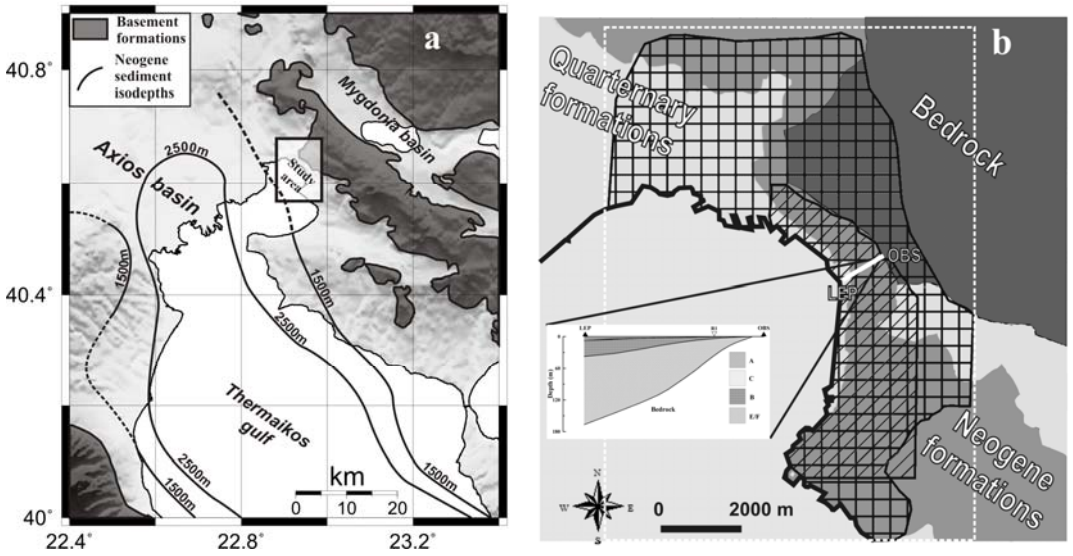

Figure 2. a) Map of the broader study area, showing the general geological features of the Axios Basin and Thermaikos Gulf. Neogene sediments isodepth lines (Lalechos and Savoyat, 1979) together with basement formations (dark areas in the map) are also shown. b) Map showing the major soil formations in the study area (broader area of the city of Thessaloniki). The bedrock formation is denoted with the dark-grey shade, while with the medium and light grey colors correspond to the Neogene and Quarternary formations, respectively. The larger (square) hatched area represents the original coverage of Apostolidis et al. (2004b) geophysical/geotechnical model (AP04), while the smaller (oblique) one the corresponding coverage of the Anastasiadis et al. (2001) geophysical/geotechnical model (AN01). The white dashed line corresponds to the limits of the modified AN01 model (see also Figure 3). The cross-section LEP-OBS is also shown together with the corresponding structure of the model formations.

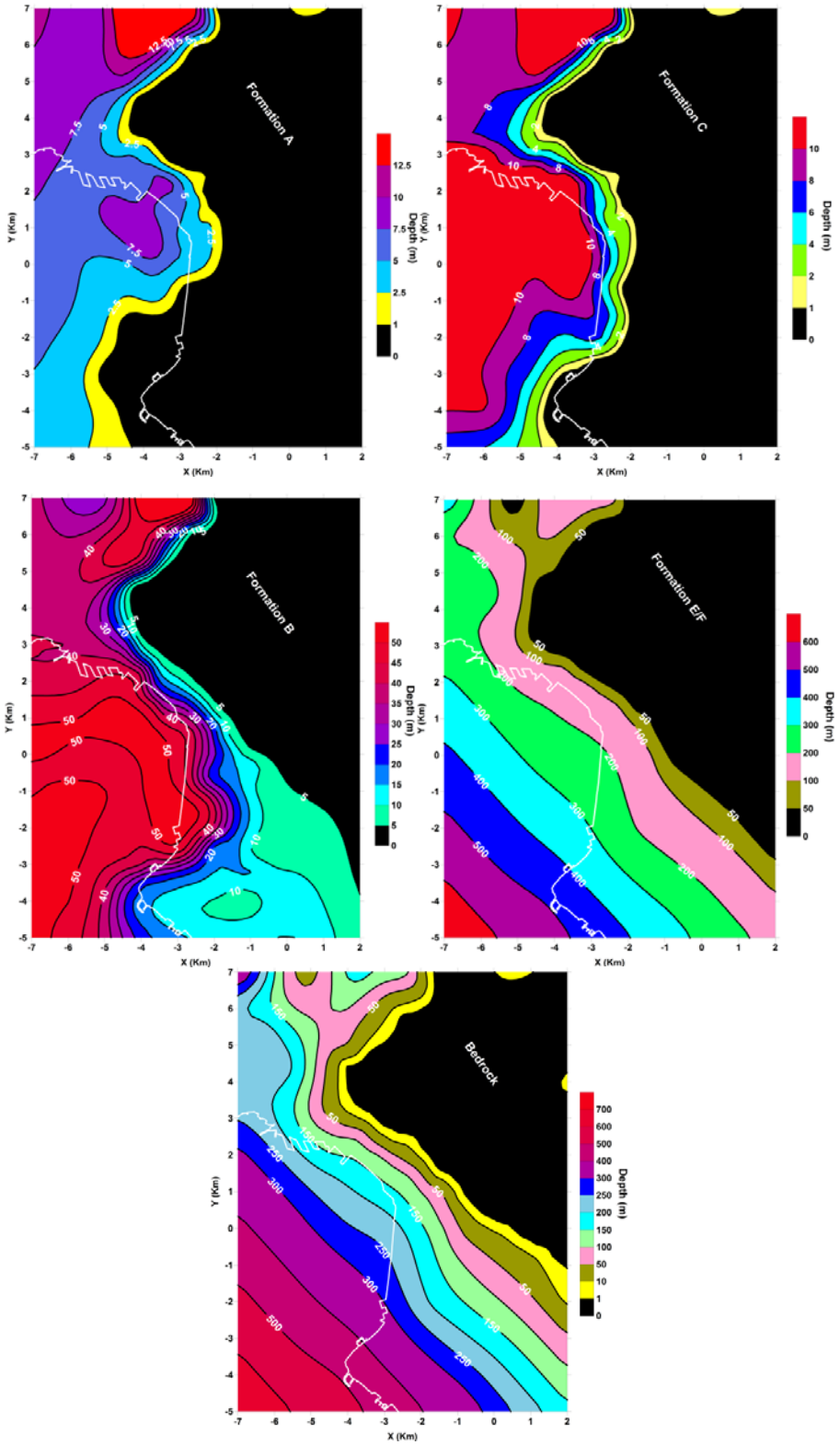

Figure 3. Depth and geometry of the soil formations of the modified AN01 geophysical/geotechnical model. The coastline is depicted with a white solid line. The area covered corresponds to the extrapolated AN01 geophysical/geotechnical model (see text for details).

[37]

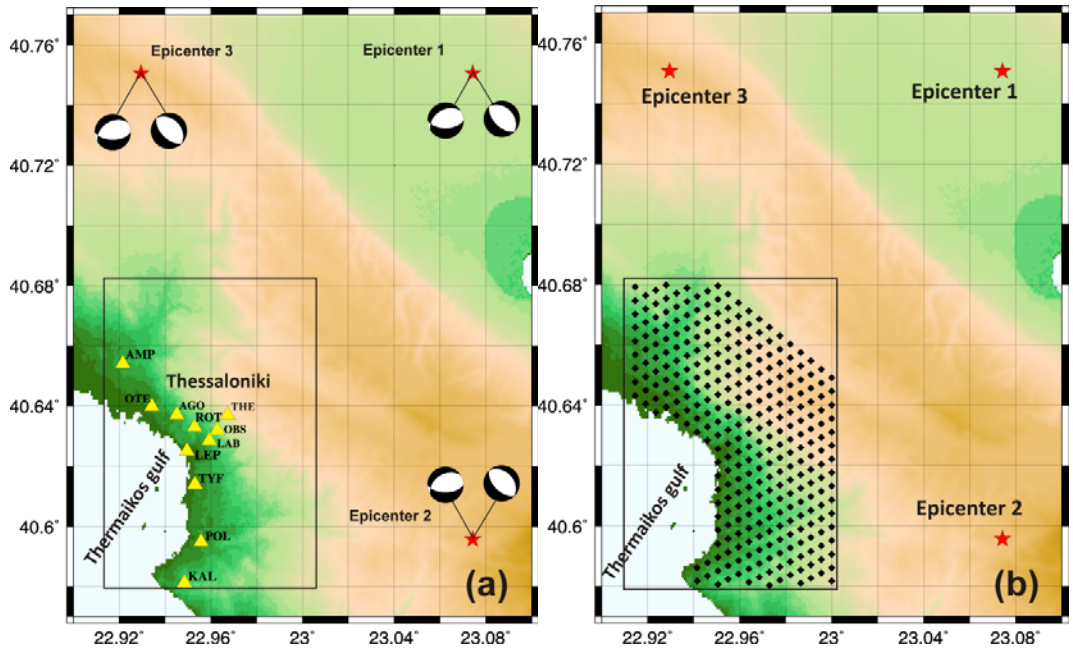

Figure 4. a) Earthquake locations used for the seismic scenarios (red stars). The focal mechanisms used for each scenario are also shown. The sites where observed data and FD synthetics are available are presented with yellow triangles. b) Grid of receivers used for studying the spatial variation of Fourier spectra for the six earthquake scenarios. The area covered corresponds to the area of the computational model, while the bounded area to the modified AN01 model (see text for details).

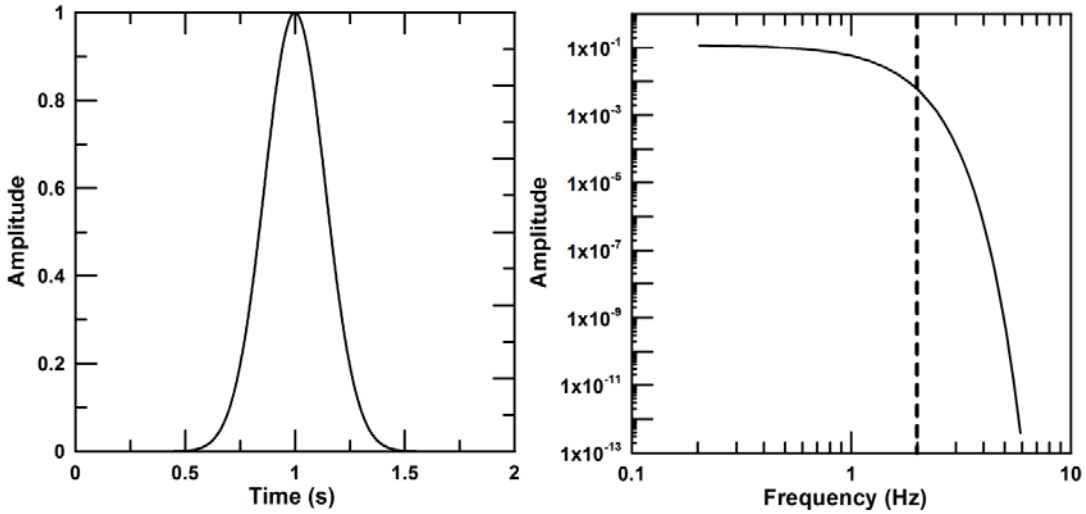

Figure 5. (Left) Source time function used for FD computations. (Right) Fourier spectrum of the source time function used in the FD simulations. The vertical dashed line denotes the maximum theoretical frequency up to which FD computations can be considered sufficiently accurate (2Hz).

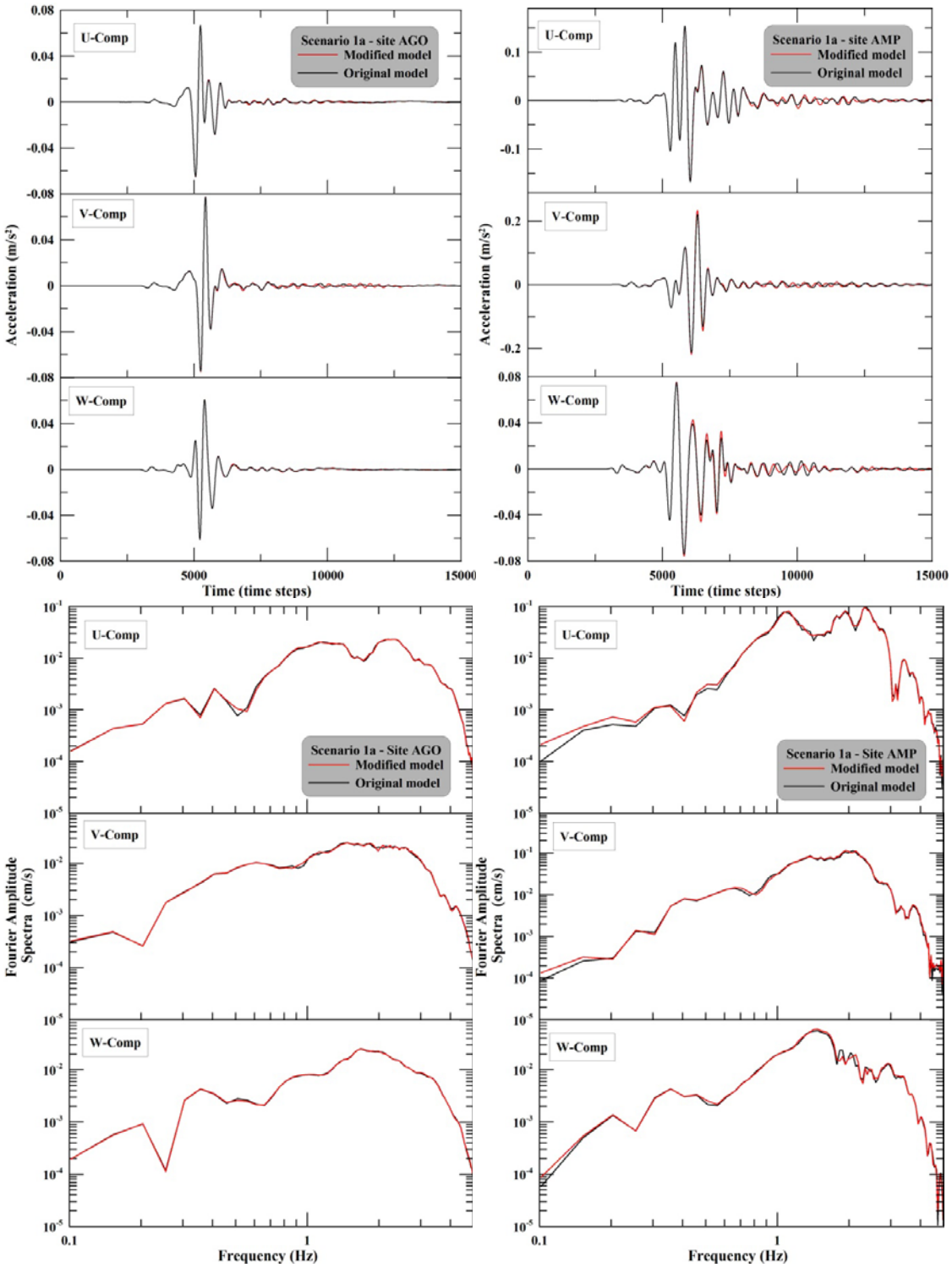

Figure 6. Top. Comparisons of 3D synthetics estimated from 2 different geophysical-geotechnical models for sites AGO and AMP and scenario 1a. Bottom. Comparisons of FAS for sites AGO and AMP.

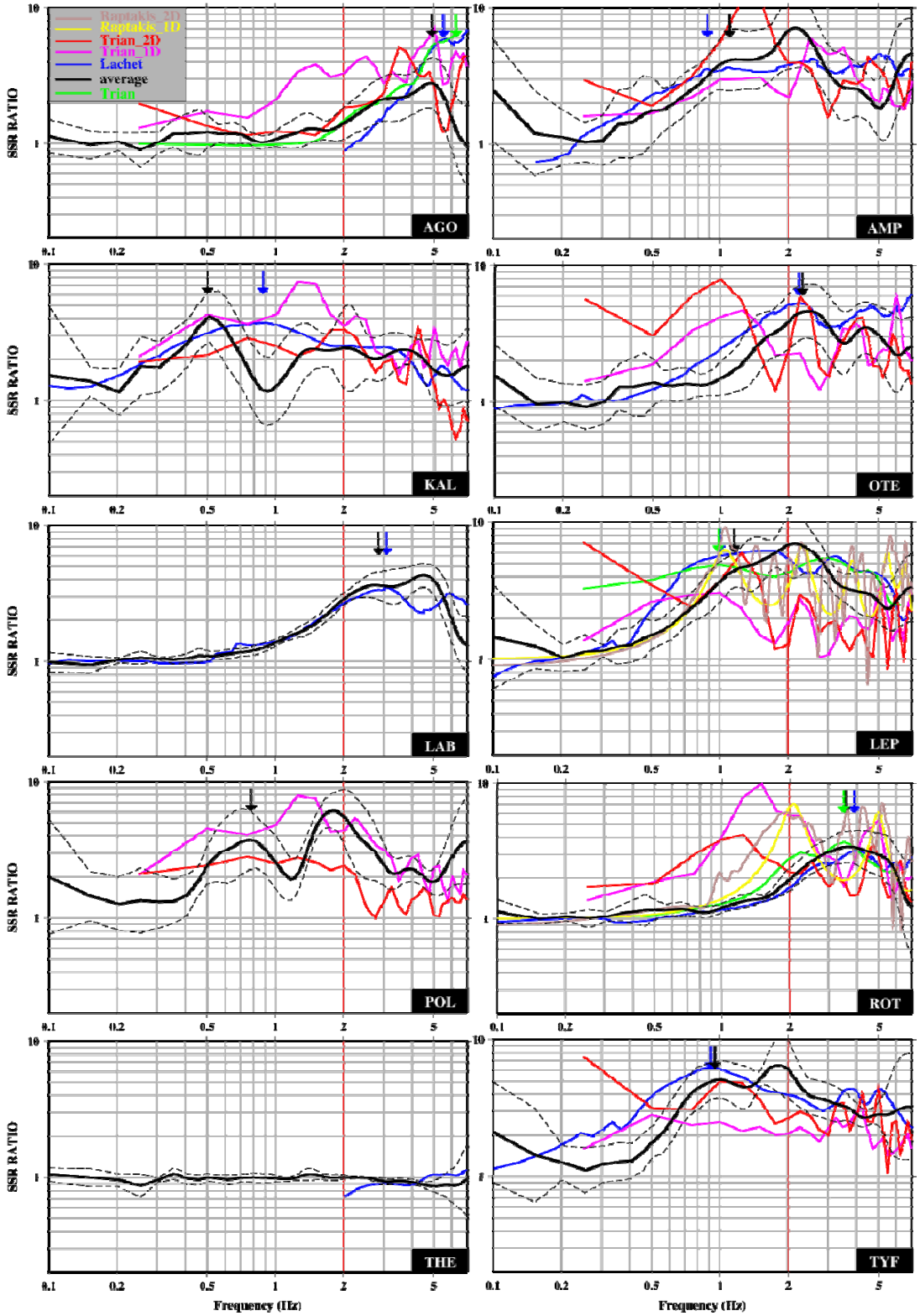

Figure 7. Average synthetic SSR curves from all six seismic scenarios (thick black line) and corresponding standard deviation (thin dashed black line) for the 10 examined sites. Empirical SSR curves derived by Lachet et al. (1996) and Triantafyllidis et al. (2004a) [41]

are denoted by the blue and green lines, respectively. Synthetic curves from 1D and 2D numerical modeling by Triantafyllidis et al. (2004b) (pink and red) and by Raptakis et al. (2004b) (yellow and brown) are also shown. The red vertical line shows the maximum frequency (f_{max}) up to which FD calculations in the present study can be considered sufficiently accurate. Colored arrows denote the fundamental frequencies of the corresponding SSR curves.

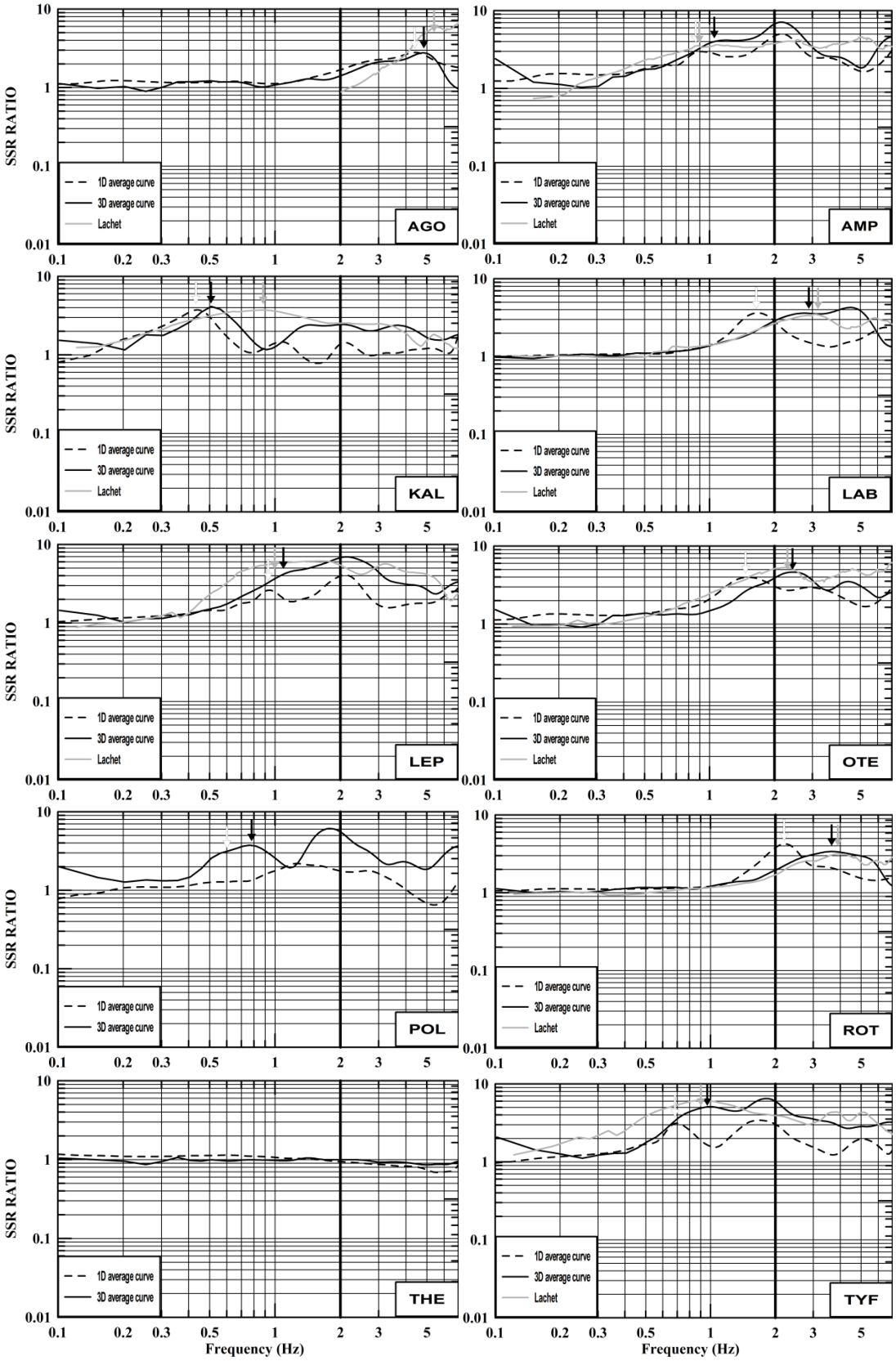
SSR RATIO
Frequency (Hz)
1D average curve
3D average curve
Lachet
AGO
AMP
KAL
LAB
LEP
OTE
POL
ROT
THE
TYF

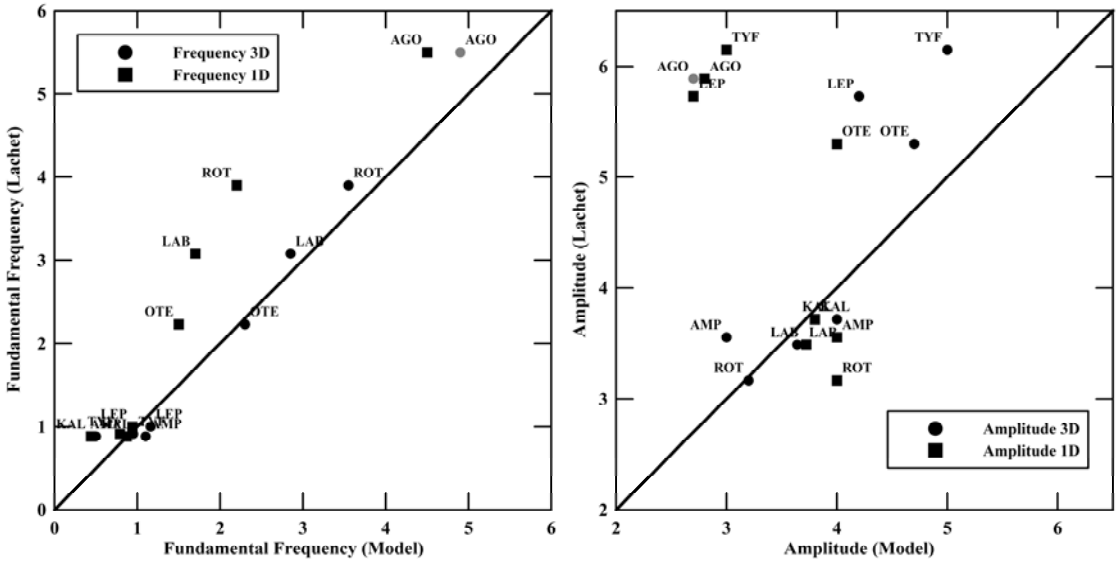

Figure 8. a) Average synthetic SSR curves from 3D (FD synthetics-solid line) and 1D (DWN synthetics-dashed line) numerical modeling for the six scenarios. The observed SSR curves from Lachet et al. (1996) are also plotted for comparison (grey line). The black vertical line corresponds to the maximum frequency (f_{max}) up to which FD calculations of the present study can be considered sufficiently accurate. Black, white and grey arrows denote the fundamental frequencies of the corresponding SSR curves. b) Comparison between the 3D (cirles) and 1D (squares) model and the empirical fundamental frequencies (left) and amplification amplitudes (right), as derived from the corresponding SSR curves. The superiority of the 3D results is evident in both cases. Station AGO, for which the 3D FD results should be considered as inaccurate, is denoted by a grey solid circle.

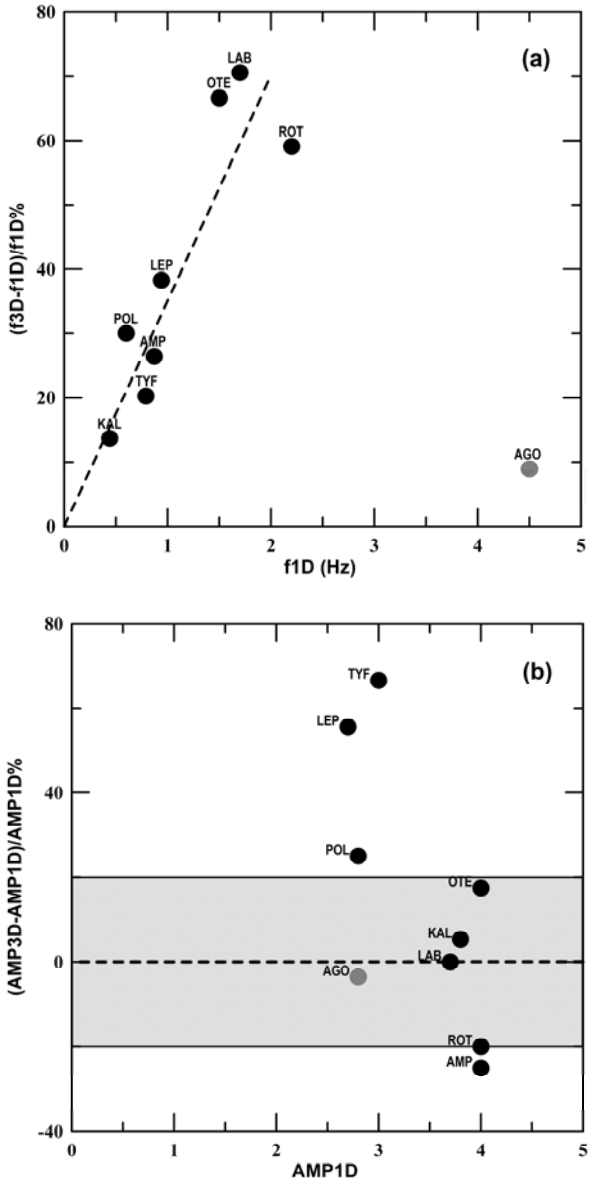

Figure 9. a) Relative variation of 3D model fundamental frequency with respect to the corresponding 1D one, plotted against the 1D fundamental frequency for each site. b) Relative variation of 3D SSR fundamental amplitudes plotted against the 1D SSR amplitude for each site. Station AGO, for which the 3D FD results should be considered as inaccurate, is denoted by a grey solid circle.

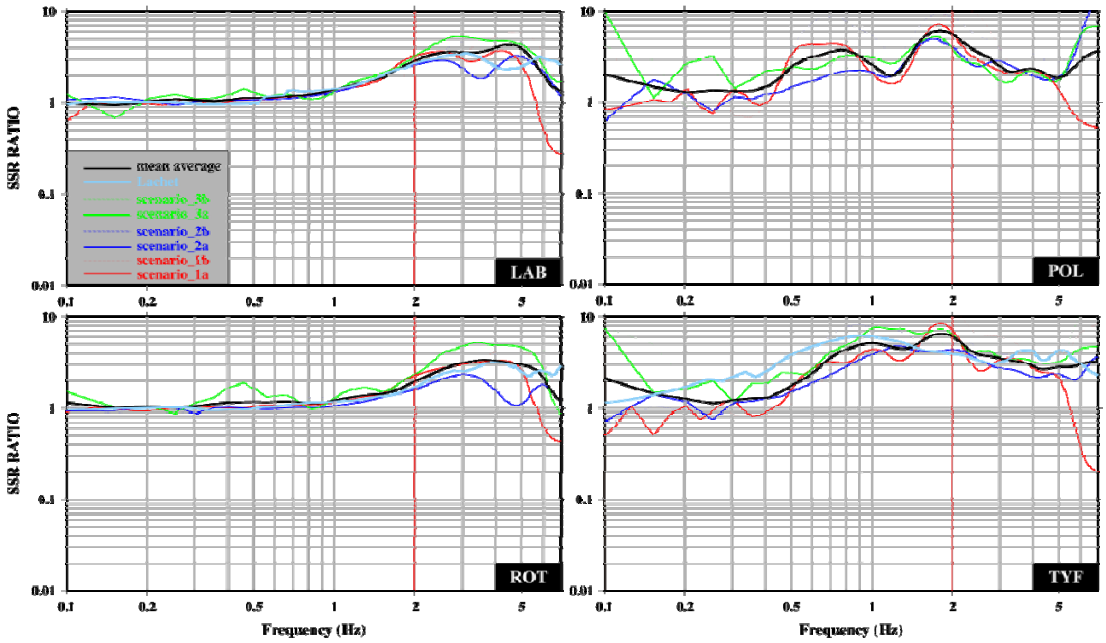

Figure 10. Synthetic SSR curves from 3D numerical modeling for the six scenarios studied (see Table 2 for each scenario parameters). Average synthetic SSR curve (black) from six scenarios and empirical SSR curves by Lachet et al. (1996) (light blue) are also shown. The red vertical line shows the maximum frequency (f_{max}) up to which FD calculations in the present study can be considered sufficiently accurate.

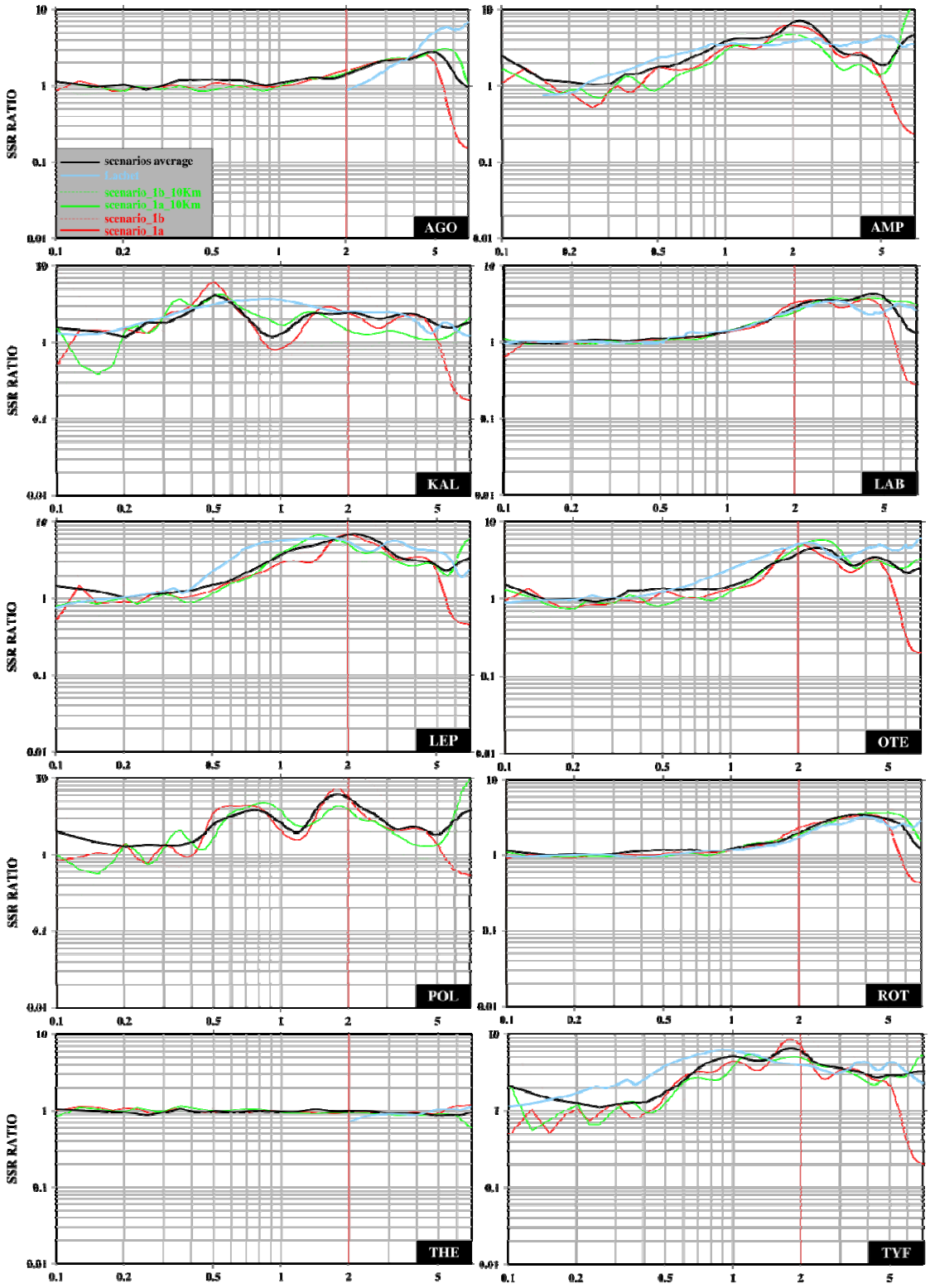

Figure 11. Synthetic SSR curves from 3D numerical modeling for scenario 1 and focal depths of 5Km (red) and 10Km (green). Average SSR curves (black) from the six scenarios and empirical SSR curves by Lachet et al. (1996) (light blue) are also plotted. [47]

The red vertical line shows the maximum frequency (f_{max}) up to which FD calculations in the present study can be considered sufficiently accurate.

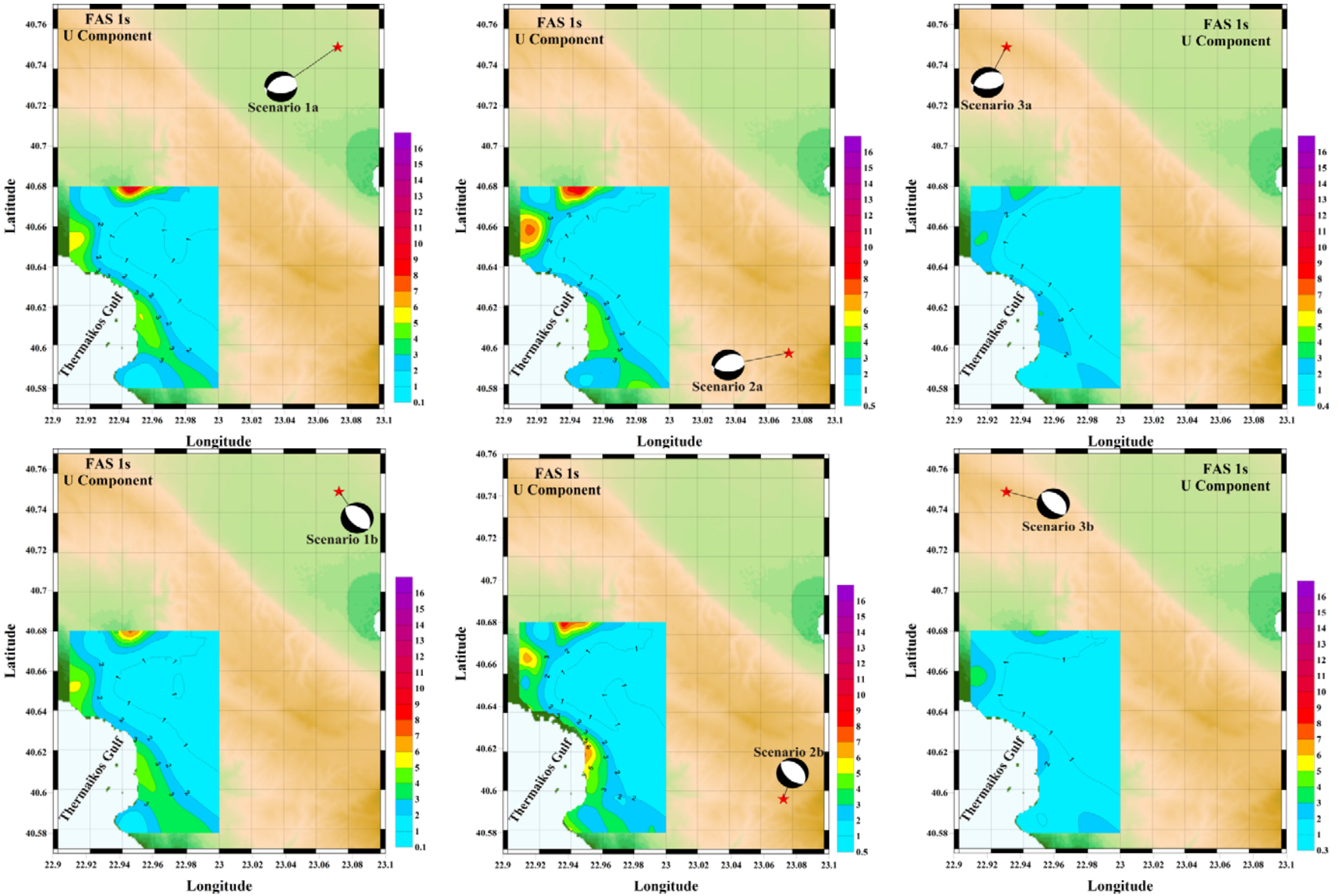

Figure 12a. Spatial variation of the average (FAS3D)/(FAS1D) ratio for the U component (N-S) for the six examined scenarios and frequency of 1Hz for the final model area and receiver configuration (Fig. 4b).

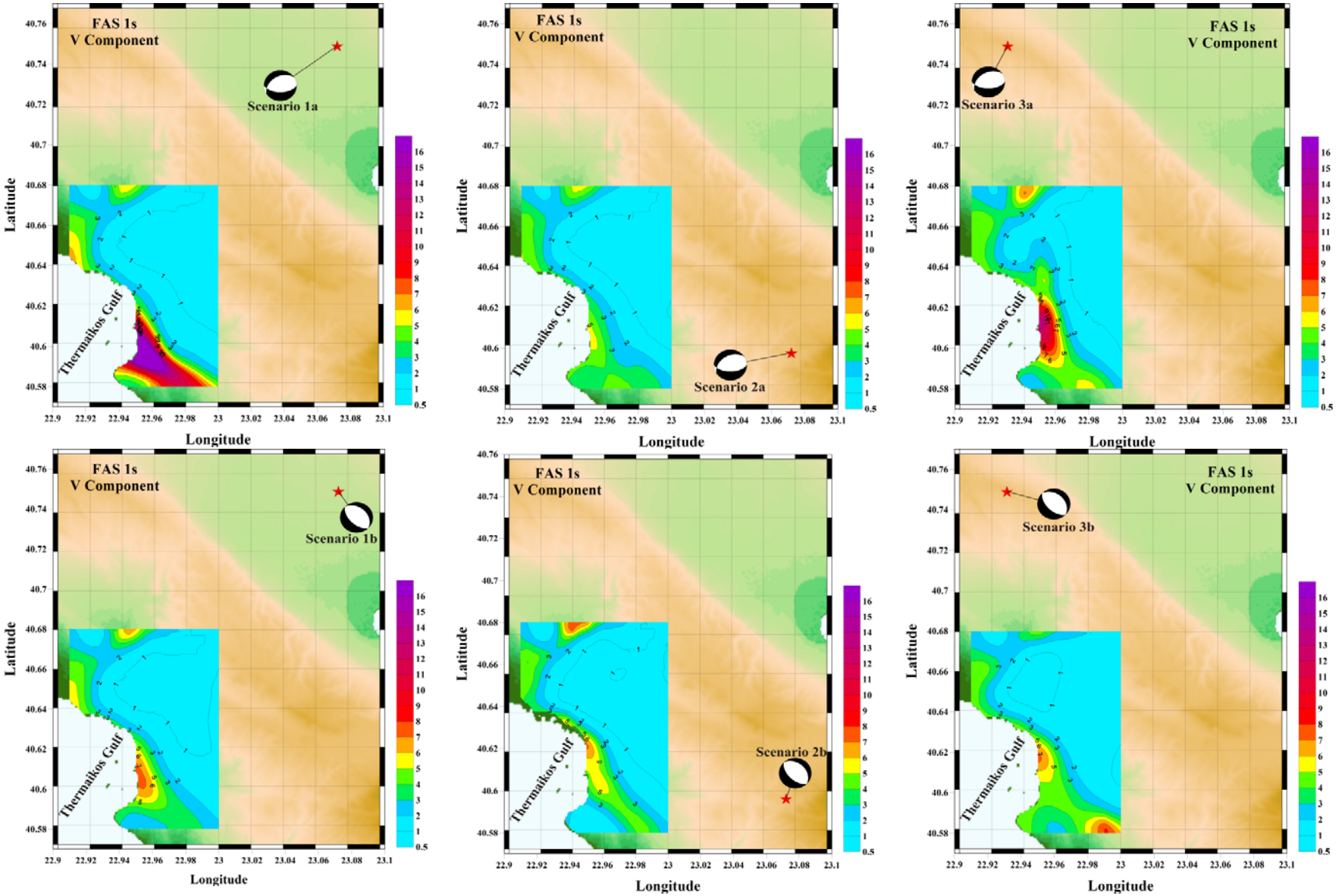

Figure 12b. Spatial variation of the average (FAS3D)/(FAS1D) ratio for the V component (E-W) for the six examined scenarios and frequency of 1Hz for the final model area and receiver configuration (Fig. 4b).

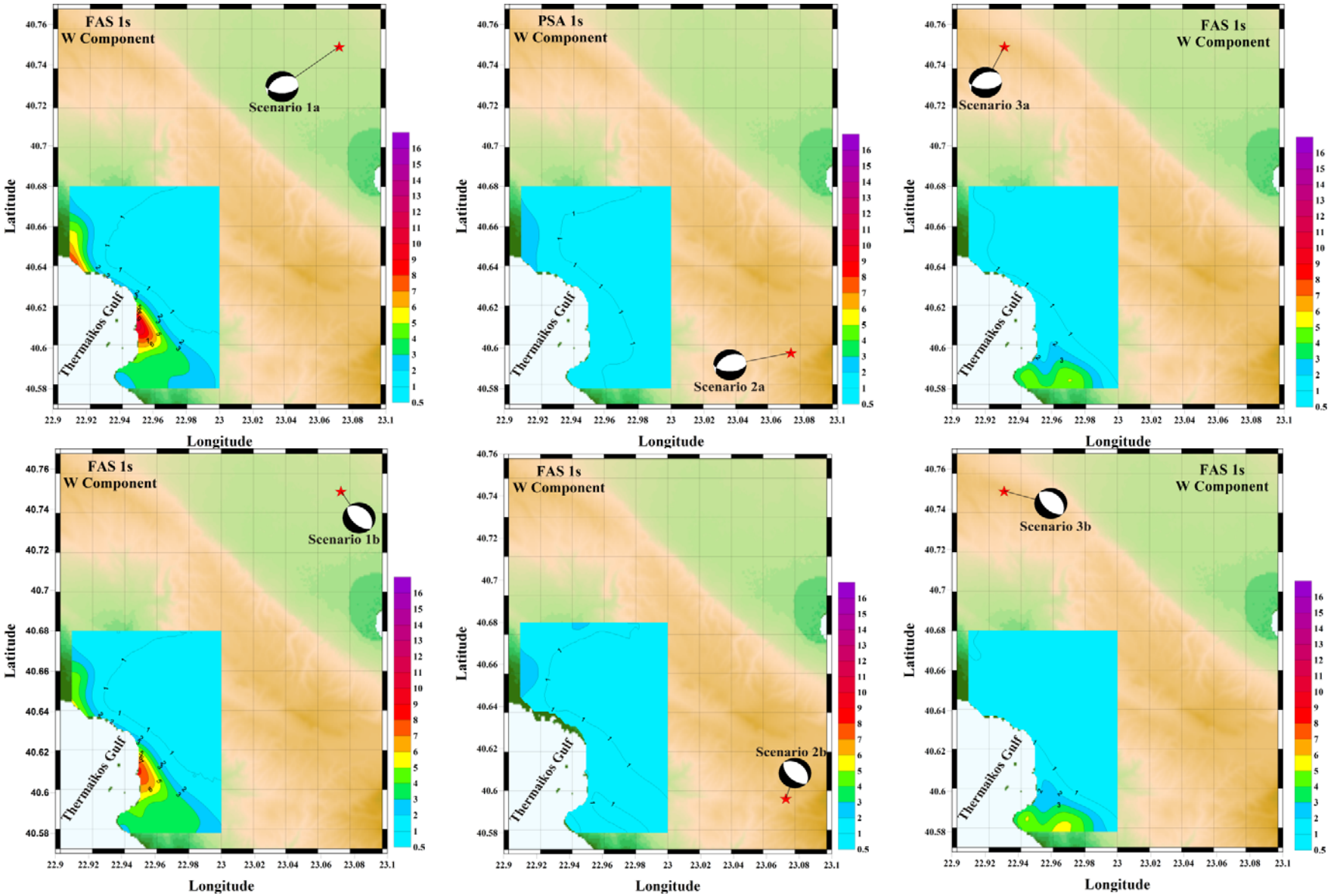

Figure 12c. Spatial variation of the average (FAS3D)/(FAS1D) ratio for the W component (Vertical) for the six examined scenarios and frequency of 1Hz for the final model area and receiver configuration (Fig. 4b).